

# Constraining dark matter late-time energy injection: decays and p-wave annihilations

Roberta Diamanti<sup>1</sup>, Laura Lopez-Honorez<sup>2</sup>, Olga Mena<sup>1</sup>, Sergio Palomares-Ruiz<sup>1</sup> and Aaron C. Vincent<sup>1</sup>

<sup>1</sup>*Instituto de Física Corpuscular (IFIC), CSIC-Universitat de València,  
Apartado de Correos 22085, E-46071 Valencia, Spain and*

<sup>2</sup>*Theoretische Natuurkunde Vrije Universiteit Brussel and The  
International Solvay Institutes Pleinlaan 2, B-1050 Brussels, Belgium*

We use the latest cosmic microwave background (CMB) observations to provide updated constraints on the dark matter lifetime as well as on p-wave suppressed annihilation cross sections in the 1 MeV to 1 TeV mass range. In contrast to scenarios with an s-wave dominated annihilation cross section, which mainly affect the CMB close to the last scattering surface, signatures associated with these scenarios essentially appear at low redshifts ( $z \lesssim 50$ ) when structure began to form, and thus manifest at lower multipoles in the CMB power spectrum. We use data from Planck, WMAP9, SPT and ACT, as well as Lyman- $\alpha$  measurements of the matter temperature at  $z \sim 4$  to set a 95% confidence level lower bound on the dark matter lifetime of  $\sim 4 \times 10^{25}$  s for  $m_\chi = 100$  MeV. This bound becomes lower by an order of magnitude at  $m_\chi = 1$  TeV due to inefficient energy deposition into the intergalactic medium. We also show that structure formation can enhance the effect of p-wave suppressed annihilation cross sections by many orders of magnitude with respect to the background cosmological rate, although even with this enhancement, CMB constraints are not yet strong enough to reach the thermal relic value of the cross section.

## I. INTRODUCTION

The temperature and polarization fluctuations of the cosmic microwave background (CMB) are sensitive to all redshifts since recombination, and the large correlation between temperature and polarization at low multipoles suggests rescattering of CMB photons at low  $z$ . Much of this can be attributed to reionization by stars, but extra energy injection into the intergalactic medium (IGM) at late times can increase correlations on large scales. As is well known, observations of the CMB set severe constraints on weakly interacting massive particles (WIMPs) models for dark matter (DM) candidates with masses in the GeV mass range and below [1–35]. In most of the studies on DM annihilations, the CMB constraints have been typically derived assuming that the annihilation cross section times the relative velocity,  $\sigma v$ , is constant, *i.e.*, s-wave annihilations (see Refs. [33, 34] for the latest results). In this case, CMB mostly constrains the new sources of ionization and heating due to the products of annihilations of the homogeneous background DM distribution around the epoch of recombination. Furthermore, in the framework of constant  $\sigma v$  and when halo formation based on N-body simulations is considered, the CMB bounds are not influenced by late-time effects such as DM clustering in structures [33] (see also Refs. [11–13, 16, 17, 20, 21, 24, 26] for other results).

In this paper, we turn our attention to two DM scenarios whose effect on the CMB is expected to be driven by late-time ( $z \lesssim 50$ ) physics. We first revisit and update the case of DM decay [1, 30] assuming that it accounts for the entire DM relic abundance. Hence, the DM lifetimes  $\tau_\chi$  considered here are assumed to be larger than the age of the Universe. The second scenario studied in this paper is the case of DM species with a velocity-suppressed annihilation cross section, specifically  $\sigma v \simeq bv^2$ . In the non-relativistic limit, the cross section may be expanded as  $\sigma v = a + bv^2 + \mathcal{O}(v^4)$ , with constant  $a$  and  $b$  which govern the s-wave and p-wave contributions, respectively. This gives rise to an averaged annihilation cross section times the relative velocity  $\langle \sigma v \rangle$  and a DM relic abundance  $\Omega_{\text{DM}} h^2$  of the following form [36–38]:

$$\langle \sigma v \rangle_{\text{FO}} = a + 6b/x_{\text{FO}} \quad \text{and} \quad \left( \frac{\Omega_{\text{DM}} h^2}{0.1} \right) \simeq 0.34 \left( \frac{x_{\text{FO}}}{\sqrt{g_*}} \right) \left( \frac{3 \times 10^{-26} \text{cm}^3/\text{s}}{a + 3b/x_{\text{FO}}} \right), \quad (1)$$

when limiting the expansion in velocity to the  $v^2$  contribution. In Eq. (1),  $x_{\text{FO}} \equiv m_\chi/T_{\text{FO}}$ , where  $m_\chi$  is the DM mass and  $T_{\text{FO}}$  is the temperature at which freeze-out (or chemical decoupling) occurs,  $g_*$  refers to the number of relativistic degrees of freedom at the time of freeze-out. Eq. (1) implies that s-wave annihilating DM requires  $\langle \sigma v \rangle_{\text{FO}} \sim 3 \times 10^{-26} \text{cm}^3/\text{s}$  in order to account for the correct cosmological abundance (see however Ref. [39] for an accurate calculation), while DM annihilating through a p-wave channel requires  $\langle \sigma v \rangle_{\text{FO}} \sim 6 \times 10^{-26} \text{cm}^3/\text{s}$ .

The rate at which DM decays or annihilations heat or ionize the baryonic component of the IGM is proportional to (see, *e.g.*, Ref. [4])

$$\mathcal{F}(z) = \frac{1}{H(z)(1+z)n_H(z)} \left( \frac{dE}{dt dV} \right)_{\text{deposited}} \quad (2)$$

where  $H(z)$  is the Hubble rate and  $n_H(z) \propto (1+z)^3$  is the density of hydrogen nuclei. In the matter dominated era, the denominator  $H(z)(1+z)n_H(z)$  suppresses energy deposition by a factor of  $(1+z)^{-11/2}$ . For the background DM component, the energy deposition rate is usually expressed through

$$\left(\frac{dE}{dt dV}\right)_{\text{deposited}} = f(z) \left(\frac{dE}{dt dV}\right)_{\text{injected}}, \quad (3)$$

where the factor  $f(z)$ , defined as

$$f(z) \equiv \frac{\text{Energy deposited into IGM at } z}{\text{Energy injected at } z}, \quad (4)$$

accounts for the fact that final-state energy can stream away with neutrinos and that energy losses by final-state electrons, positrons and photons occurs via a cascade of collisions, so they may be absorbed at later times or freely stream until the present, or until they are redshifted into a window in which the IGM is less transparent. We will return to the form of  $f(z)$  in the different scenarios in Sec. II.

Prior to structure formation, the smooth dark matter background contribution drives the energy injection rate  $(dE/dtdV)_{\text{injected}}$ . The latter is proportional to

$$\Gamma_{\text{dec}} = \frac{n_\chi}{\tau_\chi} \quad (5)$$

for DM decays. This scales as  $(1+z)^3$ , where  $n_\chi = \rho_\chi/m_\chi$  the DM number density, while for DM annihilation the injection rate is proportional to

$$\Gamma_{\text{ann}} = n_\chi^2 \langle \sigma v \rangle, \quad (6)$$

which scales as  $(1+z)^6$  for an s-wave dominated cross section. As a result, the redshift dependence of  $\mathcal{F}(z)$  goes as  $(1+z)^{1/2}$  for s-wave DM annihilation cross sections whereas for DM decays, it goes as  $(1+z)^{-5/2}$ . This explains why DM decays are expected to affect CMB at later times than s-wave DM annihilations. In the case of p-wave suppressed DM annihilation cross sections, the two extra powers of  $v$  in  $\langle \sigma v \rangle$  redshift with time as  $(1+z)^2$  so that the background injected energy rate goes as  $\Gamma_{\text{ann}} \propto (1+z)^8/(1+z_{\text{KD}})^2$ , where  $z_{\text{KD}}$  is related to the time of DM kinetic decoupling — when local thermal equilibrium is not maintained any more by scattering with Standard Model (SM) particles — and which typically occurs well before recombination  $z_{\text{KD}} \gg z_{\text{rec}}$ . This will be explored in greater detail in Sec. II B. Although such a dependence appears to severely suppress the impact of p-wave DM annihilations on CMB photons at all times, this discussion only applies for the background contribution. In contrast, we will show that the enhancement at late times of the  $n_\chi^2$  and  $v^2$  factors provided by the formation of DM halos dominates by many orders of magnitude over the background contribution. In both the case of DM decays and p-wave DM annihilations, late-time contributions to rescattering of CMB photons would mainly manifest as a modification to the low-multipole polarization spectrum of the CMB, albeit for different physical reasons.

In Sec. II, after briefly characterizing the time-dependence of energy injection into the IGM in general, we further describe our treatment of energy injection from DM decay (Sec. II A) and p-wave annihilation (Sec. II B). In order to obtain the limits for both scenarios we use the latest available CMB data, including the recent Planck data [34], the nine-year temperature and polarization data release from the Wilkinson Microwave Anisotropy Probe (WMAP) collaboration [40] and the high-multipole CMB data released by the South Pole Telescope (SPT) [41, 42] and by the Atacama Cosmology Telescope (ACT) [43] experiments. We also add a prior on the Hubble constant,  $H_0$ , from the Hubble Space Telescope (HST) [44] and from Baryon Acoustic Oscillation (BAO) measurements from different surveys [45–48]. Finally, we also use the determination of the IGM temperature from Lyman- $\alpha$  observations [49], which significantly improves the limits. Our results are presented and discussed in Sec. III and we conclude in Sec. IV.

## II. ENERGY INJECTION SCENARIOS

Final-state energy produced by DM decays or annihilations can stream away in the form of neutrinos, while the daughter photons, electrons and positrons may be absorbed at later times into the IGM via different processes, which include photoionization, Coulomb scattering, Compton processes, bremsstrahlung and recombination. These effects can be written in terms of a transfer function  $T_i(z', z, E)$  for each channel  $i = \{e^\pm, \gamma\}$ , which describes the fraction of the original particle's energy deposited into the IGM at a redshift  $z$ , for a redshift of injection  $z'$  and an initial energy  $E$ , per logarithmic redshift bin  $d \ln(1+z)$ . In this case, “deposition” simply means that the particles hit

some threshold energy, below which their absorption into the IGM as heat or ionization energy can be considered instantaneous.

This has been computed by several authors [15, 19, 25] with Monte Carlo codes which track the evolution of “primary” particles and of their “secondary” daughters in an expanding Universe. Tabulated  $T_i(z', z, E)$  have been made public<sup>1</sup> by Ref. [28]. Eq. (4) corresponds to a normalized integral over all previously injected energy, which can be written in a general form valid for different scenarios, as

$$f_\alpha(z, m_\chi) = \frac{\sum_i \int E dE \int dz' T_i(z', z, E) \frac{dN_i(E, m_\chi)}{dE dz'}}{\sum_i \int E dE \frac{dN_i(E, m_\chi)}{dE d \ln(1+z)}}, \quad (7)$$

where  $\frac{dN_i(E, m_\chi)}{dE d \ln(1+z)}$  is the spectrum of injected particles, per comoving volume, as a function of energy and redshift for a given DM mass  $m_\chi$ . Omitting the redshift-independent and energy-independent proportionality factors, we have:

$$\frac{dN_i(E, m_\chi)}{dE d \ln(1+z)} \propto \frac{\Gamma_\alpha(z)}{(1+z)^3 H(z)} \frac{dN_i(E, m_\chi)}{dE}, \quad (8)$$

where  $\frac{dN_i(E, m_\chi)}{dE}$  is the energy spectrum of final-state particles per DM annihilation or decay and  $\Gamma_\alpha$  is defined in Eqs. (5) and (6) and scales as  $(1+z)^3$ ,  $(1+z)^6$  and  $(1+z)^8$  for decaying, s-wave and p-wave annihilating dark matter species, respectively. The energy spectrum of decays and annihilations into  $e^+e^-$  and  $\mu^+\mu^-$  is computed as in Ref. [33] and for the  $\tau^+\tau^-$  channel we use the publicly available results<sup>2</sup> of Refs. [50, 51].

In the present work, we use the  $T_i(z', z, E)$  functions obtained in Ref. [28]. Note, however, that these results neglect heating from proton and antiproton final-state particles, which may account for up to 20% of the deposited energy for some channels [31]. This effect would change the CMB bounds on DM at the 10% level. It was also recently pointed out that errors in the standard computation of  $f(z)$  may introduce systematic uncertainties that could weaken constraints [52], although in practice the effects of these on energy injection bounds turn out to be small [35].

### A. DM decays

In general, the decay of unstable particles may affect the redshift of recombination, as well as reionization at low redshift (see *e.g.*, Refs. [1, 5, 7, 8, 23, 28, 30, 53, 54]). The rate of energy per unit volume liberated by such an unstable cosmological species  $\chi$  reads

$$\left( \frac{dE}{dt dV} \right)_{\text{injected}} = (1+z)^3 \frac{\phi_{\text{SM}}}{\tau_\chi} \Omega_\chi \rho_c, \quad (9)$$

and depends linearly on its number density,  $n_\chi = \Omega_\chi \rho_c (1+z)^3 / m_\chi$ , where  $\Omega_\chi$  is the contribution of  $\chi$  to the critical density  $\rho_c$ , and  $\phi_{\text{SM}}$  is the fraction of its mass that goes to into SM particles when decaying (while  $(1 - \phi_{\text{SM}})$  would go to some other dark sector species). Here we assume that  $\chi$  accounts for all the DM such that  $\Omega_\chi = \Omega_{\text{DM},0}$ , it fully decays to SM particles ( $\phi_{\text{SM}} = 1$ ) and has a lifetime  $\tau_\chi \gg t_U$  where  $t_U = 4.34 \times 10^{17}$  s is the age of the Universe. To consider particles with significantly shorter lifetimes, one would include an exponential factor in (9) to parametrize the species' depletion.

In practice, we have used `CosmoRec` package [18, 55–60] in order to compute the changes in the ionization history. `CosmoRec` includes a subroutine that modifies the evolution equations for the IGM temperature and for the net ionization rate from the ground states of neutral hydrogen and helium, which depends on the energy deposition by the DM. In the case of DM decays, inspired by Ref. [18], we use the parametrization

$$\left( \frac{dE}{dt dV} \right)_{\text{deposited}} = f_{\text{eff,dec}}(m_\chi) \epsilon_{\text{dec}} n_H(z) \text{ eV/s} \quad \text{with} \quad \epsilon_{\text{dec}} = 7.2 \times 10^{-14} \left[ \frac{10^{23} \text{ s}}{\tau_\chi} \right] \left[ \frac{\Omega_{\text{DM},0} h^2}{0.13} \right], \quad (10)$$

where  $n_H(z) = 1.9 \times 10^{-7} \text{ cm}^{-3} (1+z)^3$  is approximately the number density of hydrogen nuclei in the Universe.

Analogously to Ref. [33], we define an effective  $f_{\text{dec}}(z, m_\chi)$  averaged over redshift which depends on the DM mass only and allows us to simplify the numerical analysis. This allows for constraints computed with a given final state

<sup>1</sup> <http://nebel.rc.fas.harvard.edu/epsilon/>

<sup>2</sup> <http://www.marcocirelli.net/PPPC4DMID.html>

and  $z$ -dependence to be rescaled for each value of the DM mass. However, the redshift dependence of  $f_{\text{dec}}(z, m_\chi)$  in the case of decays is much more pronounced than for annihilations and, for masses above  $\sim 1$  GeV, it is not possible to accurately reproduce the free electron fraction  $x_e(z)$  with a constant  $f_{\text{eff}}(m_\chi)$  for each DM mass, in turn causing effects at intermediate redshifts to be underestimated when using the parametrization in Ref. [33]. Nevertheless, the injection of additional energy broadens the last scattering surface by increasing the residual ionization, without slowing recombination [4]. This is reflected in the visibility function,  $\tilde{g}(z) = -\tau' e^{-\tau}$ , where  $\tau$  is the optical depth and  $'$  indicates the derivative with respect to the conformal time,  $\eta$ . Whereas around recombination, the visibility function is approximately the same with or without the small energy injection from DM, below  $z_{\text{max}} \simeq 600 - 800$  (depending on the decay channel and lifetime), energy injection creates a longer tail on  $\tilde{g}(z)$ . At these times, the optical depth is very small, so the exponential factor in  $\tilde{g}(z)$  is approximately one, and the visibility function is  $\tilde{g}(z) \simeq -\tau' \propto x_e(z)(1+z)^2$ . By using the redshift dependence of  $x_e(z)$  [33], we can define  $\tilde{g}_{\text{eff}}$  with  $f_{\text{eff,dec}}(m_\chi)$  determined by imposing  $\int_{\eta(z_{\text{max}})}^{\eta(0)} d\eta \tilde{g}(\eta) = \int_{\eta(z_{\text{max}})}^{\eta(0)} d\eta \tilde{g}_{\text{eff}}(\eta)$ , which reads

$$f_{\text{eff,dec}}(m_\chi) = \frac{\int_{z_{\text{max}}}^0 \frac{(1+z)^2}{H(z)} dz \int_\infty^z \frac{\Gamma_{\text{dec}}(z')}{(1+z')^4 H(z')} f_{\text{dec}}(z', m_\chi) dz'}{\int_{z_{\text{max}}}^0 \frac{(1+z)^2}{H(z)} dz \int_\infty^z \frac{\Gamma_{\text{dec}}(z')}{(1+z')^4 H(z')} dz'} , \quad (11)$$

where  $\Gamma_{\text{dec}}$  is defined in Eq. (5). We have checked that for  $\chi \rightarrow e^+e^-$ ,  $f_{\text{eff,dec}}(m_\chi)$  leads to constraints within 5% of those computed using the full  $f_{\text{dec}}(z, m_\chi)$ , for values of  $m_\chi$  sampled in the full range considered, between  $\sim 2$  MeV and 1 TeV, using  $z_{\text{max}} = 800$ . For decays to  $\mu^+\mu^-$  and  $\tau^+\tau^-$ , constraints obtained with Eq. (11) are within 20% and 15% of those obtained with  $f(z, m_\chi)$ , respectively. In both cases we use  $z_{\text{max}} = 600$ . Tabulated values of  $f_{\text{eff,dec}}(m_\chi)$  for these three decay channels are given in Appendix A<sup>3</sup>.

In Fig. 1, we show the resulting free electron fraction  $x_e(z)$  as a function of the redshift from the recombination period with and without extra energy injection by DM. The light blue band is shown for reference and corresponds to the Planck 95% confidence level (CL) determination<sup>4</sup> of the optical depth to reionization  $\tau_{\text{reio}} = 0.089^{+0.027}_{-0.024}$  (in the absence of a DM contribution). In the left panel of Fig. 1, the three other curves illustrate the impact on  $x_e(z)$  of a 50 MeV DM candidate decaying 100% into electron/positron pairs with three different lifetimes. In addition to the DM contribution, a simplified model for reionization from stars at  $z_{\text{reio}} = 7$ , as implemented in the CAMB code [61], has been taken into account in each case (in the standard case in which reionization is induced by star formation only, current cosmological measurements indicate  $z_{\text{reio}} \sim 11$  [34]). However, let us note that for our Monte-Carlo-generated constraints, we leave the redshift of reionization as a free parameter, as indicated below. As expected, the effect of long-lived decaying DM becomes important at late times and, as we shall illustrate, lifetimes such as  $\tau_\chi = 10^{25}$  s are clearly excluded by CMB data for a 50 MeV DM candidate decaying into  $e^+e^-$ .

## B. DM p-wave annihilations

The second scenario that we examine involves DM annihilating predominantly through p-wave processes, *i.e.*,  $\sigma v \simeq b v^2$  with constant  $b$ . In this case, the total deposited energy is parametrized as

$$\left( \frac{dE}{dV dt} \right)_{\text{deposited}} = \left[ \left( \frac{1+z}{1+z_{\text{ref}}} \right)^2 f_{\text{p}}(z, m_\chi) + g_{\text{p}}(z, m_\chi, v_{\text{ref}}) \right] (1+z)^6 \rho_\chi^2 \frac{\sigma v_{\text{ref}}}{m_\chi} , \quad (12)$$

where the first term in the square brackets accounts for the background DM contribution and the second term for the halo contribution, with  $\rho_\chi = \Omega_{\text{DM},0} \rho_c$ . We have written the p-wave suppressed annihilation cross section  $\langle \sigma v \rangle$  as  $\langle \sigma v \rangle = \sigma v_{\text{ref}} \langle v^2 \rangle / v_{\text{ref}}^2$ , defining an arbitrary reference velocity  $v_{\text{ref}}$ . The background component is proportional to  $f_{\text{p}}(z, m_\chi)$ , defined in Eq. (7) with  $\Gamma_\alpha$  of Eq. (6) scaling as  $(1+z)^8$ . We made use of the fact that, after the time of kinetic decoupling, the temperature of non-relativistic species in an expanding Universe goes as  $T \propto (1+z)^2$  so that, using equipartition of energy,  $\langle v^2 \rangle$  is related to  $v_{\text{ref}}$  or equivalently  $z_{\text{ref}}$  (at which  $\sigma v_{\text{ref}}$  is evaluated) through

$$\frac{\langle v^2 \rangle}{v_{\text{ref}}^2} = \frac{T_\chi(z)}{T_{\text{ref}}} = \left( \frac{1+z}{1+z_{\text{ref}}} \right)^2 . \quad (13)$$

In this work, we present our results for  $v_{\text{ref}} = 100$  km/s, since that is the order of the dispersion velocity of DM in halos today and is thus the relevant quantity for comparison with indirect DM searches. In the case of the halo

<sup>3</sup> Let us note that the quoted values for  $z_{\text{max}}$  are not obtained from a fit to  $f_{\text{dec}}(z, m_\chi)$ , but are educated choices which provide accurate results.

<sup>4</sup> [http://www.sciops.esa.int/SYS/WIKI/uploads/Planck\\_Public\\_PLA/3/32/Grid\\_limit95.pdf](http://www.sciops.esa.int/SYS/WIKI/uploads/Planck_Public_PLA/3/32/Grid_limit95.pdf) baseline model 2.1

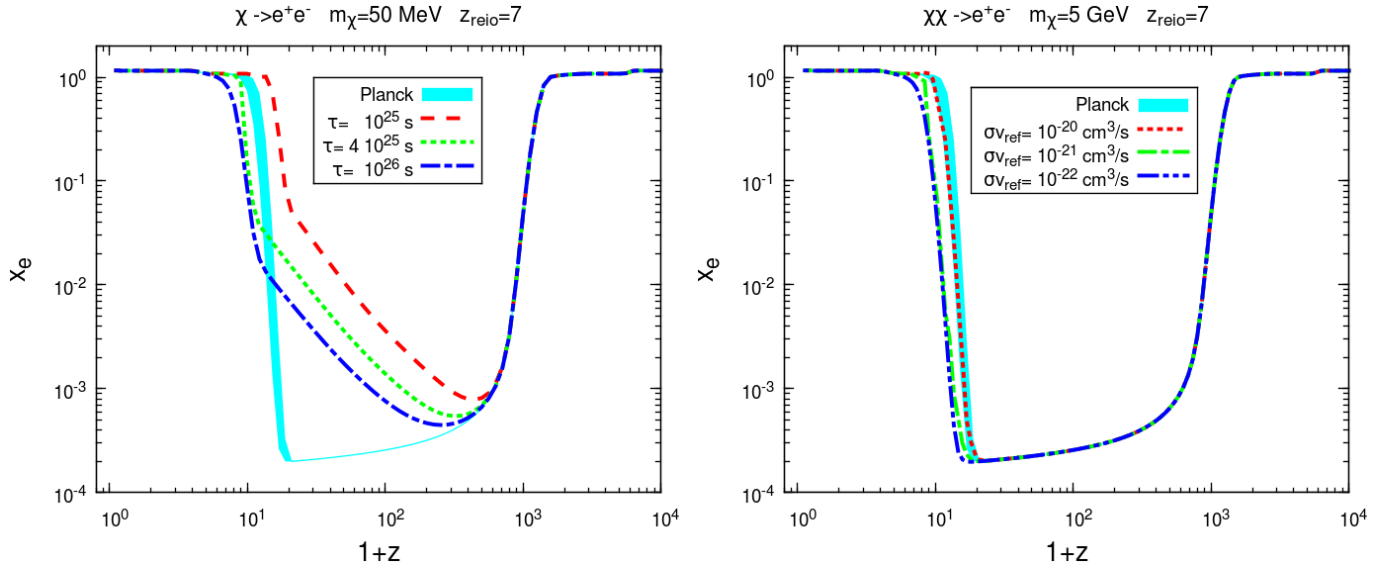


FIG. 1. The free electron fraction  $x_e$  as a function of redshift  $1+z$  in the case of DM decays (left) and  $p$ -wave annihilations (right). Both scenarios can enhance ionization at late times, due to the redshift dependence of their energy release.

contribution, the relevant  $\langle v^2 \rangle / v_{\text{ref}}^2$  factor has been absorbed into the definition of  $g_p(z, m_\chi, v_{\text{ref}})$  and will be given explicitly in Sec. II B 2.

### 1. Background DM contribution

One can estimate  $z_{\text{ref}}$ , the redshift at which the root mean square velocity  $v_{\text{rms}} \equiv \sqrt{\langle v^2 \rangle}$  of the background DM is equal to  $v_{\text{ref}}$ , as a function of the redshift of kinetic decoupling  $z_{\text{KD}}$  and the corresponding temperature  $T_\chi(z_{\text{KD}}) = T_{\text{KD}}$ . Using Eq. (13) and equipartition of energy for an ideal gas,

$$1 + z_{\text{ref}} = \frac{v_{\text{ref}}}{c} (1 + z_{\text{KD}}) \left( \frac{m_\chi}{3 T_{\text{KD}}} \right)^{1/2}. \quad (14)$$

Furthermore, one can express  $z_{\text{KD}}$  in terms of  $T_{\text{KD}}$  and the CMB temperature by using the fact that DM was in thermal equilibrium with the CMB at the time of kinetic decoupling,

$$1 + z_{\text{KD}} = \frac{T_{\text{KD}}}{T_{\text{CMB},0}} \simeq 4.2 \times 10^9 \left( \frac{T_{\text{KD}}}{\text{MeV}} \right), \quad (15)$$

where  $T_{\text{CMB},0} = 0.238$  MeV is the temperature of the CMB today. Combining Eqs. (14) and (15),

$$1 + z_{\text{ref}} \simeq 2.56 \times 10^7 \left( \frac{T_{\text{KD}}}{\text{MeV}} \right)^{1/2} \left( \frac{m_\chi}{\text{GeV}} \right)^{1/2}. \quad (16)$$

The temperature of kinetic decoupling is model-dependent and has been computed by several authors on a case-by-case basis [62–76]. Of interest for the annihilating DM scenario considered here, Ref. [76] considered fermionic DM candidates annihilating into SM leptons through effective interactions suppressed by an energy scale  $\Lambda$  that give rise to  $p$ -wave suppressed annihilation cross section for scalar type interactions. In this case, assuming that the DM mass is much larger than the final-state lepton mass, Ref. [76] obtained a temperature of kinetic decoupling

$$T_{\text{KD}} = 0.69 \frac{g_{\text{eff}}^{1/8}}{g_\chi^{1/4}} \Lambda \left( \frac{48\pi m_\chi}{M_{\text{pl}}} \right)^{1/4} \simeq 2.02 \text{ MeV} \left( \frac{m_\chi}{\text{GeV}} \right)^{3/4}. \quad (17)$$

For the second equality above, we have taken  $g_{\text{eff}} \simeq 100$  (relativistic degrees of freedom at  $T_{\text{KD}}$ ),  $g_\chi = 2$  (internal degrees of freedom of the DM particle) and  $\Lambda$  was chosen so that the annihilation cross section at the time of freeze-out matches  $\langle \sigma v \rangle = 6 \times 10^{-26} \text{ cm}^3 \text{ s}^{-1}$ . The value of  $T_{\text{KD}}$  obtained by Ref. [76] considering the case of vector type

interactions giving rise to an s-wave annihilation cross section only differs from the p-wave case by a few percent. As an additional example, the kinetic decoupling temperature for neutralino DM from Ref. [64] is estimated to be

$$T_{\text{KD}} \sim \text{MeV} \left( \frac{m_\chi}{\text{GeV}} \right)^{2/3}. \quad (18)$$

Thus, in general, kinetic decoupling occurs at a later stage than chemical freeze-out, which takes place at  $T_{\text{FO}} \simeq m_\chi/20$ . Combining Eq. (17) with Eq. (16), one can see that the background contribution in Eq. (12) is severely suppressed at redshifts  $z \sim 10^3$  and below, even for  $f_{\text{p}}(z, m_\chi) = 1$ . In fact, the suppression of the background contribution at the epoch of recombination, combined with the velocity enhancement at late times in DM structures, makes the halo contribution  $g_{\text{p}}(z, m_\chi, v_{\text{ref}})$  in Eq. (12) dominate the energy deposition history by many orders of magnitude, in contrast to the case of s-wave annihilations. This is discussed in the following section.

## 2. Halo contribution

At late times, the formation of halos not only enhances the DM average squared number density  $\langle n_\chi^2 \rangle$ , but also the average of the square of the DM particles relative velocity,  $\langle v^2 \rangle$ . This is simply due to a transfer of gravitational potential energy into kinetic energy of the individual particles that make up each halo. In order to illustrate the importance of the halo contribution, we define an effective DM density

$$\rho_{\text{eff,s}} = \rho_\chi (1+z)^3 (1 + G_{\text{s}}(z))^{1/2}, \quad (19)$$

for s-wave dominated annihilation [16], and analogously

$$\rho_{\text{eff,p}} = \rho_\chi (1+z)^3 \left( \left( \frac{1+z}{1+z_{\text{ref}}} \right)^2 + G_{\text{p}}(z, v_{\text{ref}}) \right)^{1/2}, \quad (20)$$

for p-wave dominated annihilation.

Both effective DM densities depend on a dimensionless halo contribution defined as

$$G_{\text{s}}(z) \equiv \frac{1}{\rho_\chi^2} \frac{1}{(1+z)^6} \int dM \frac{dn(M, z)}{dM} \int_0^{r_\Delta} dr 4\pi r^2 \rho_{\text{halo}}^2(r), \quad (21)$$

for s-wave annihilation [33], and as

$$G_{\text{p}}(z, v_{\text{ref}}) \equiv \frac{1}{\rho_\chi^2} \frac{1}{(1+z)^6} \int dM \frac{dn(M, z)}{dM} \int_0^{r_\Delta} dr 4\pi r^2 \frac{\langle v^2(r) \rangle}{v_{\text{ref}}^2} \rho_{\text{halo}}^2(r), \quad (22)$$

for p-wave annihilation. In both cases,  $dn(M, z)/dM$  is the halo mass function and  $\rho_{\text{halo}}(r)$  is the density profile of each individual halo with virial radius  $r_\Delta$ . Here we use the results of N-body simulations from Ref. [77] for the halo mass function and from Ref. [78] to obtain the relation of the concentration parameter to the halo mass assuming a Navarro, Frenk and White (NFW) DM density profile [79] for each individual halo. In Eq. (22), the extra factor of  $\langle v^2(r) \rangle / v_{\text{ref}}^2$  accounts for the halo-dependent velocity boost. The angular brackets represent an average over the square of the DM velocity distribution in the halo, which we take to follow a Maxwell-Boltzmann distribution.

The energy injected into the IGM at a given redshift from the annihilation of DM particles, both by the background and the halo DM contributions, depends on  $\rho_{\text{eff}}^2$ , which is depicted in Fig. 2 for s-wave and p-wave annihilations. This figure clearly illustrates that, while the overall energy injected from DM is smaller in the p-wave case, the relative contribution from halos is much larger than in the s-wave case, providing a potentially distinct imprint in the CMB power spectrum.

Let us note that the changing fraction of the Universe's DM that is contained in halos,  $\phi_{\text{halo}}(z)$ , is defined as  $\int dM M dn/dM = \phi_{\text{halo}}(z) \rho_\chi(z)$ . To account for this, the first and second terms in parentheses in Eqs. (19–20) should respectively be multiplied by  $(1 - \phi_{\text{halo}})^2$  and  $\phi_{\text{halo}}$ . However,  $G$  is a rapidly growing function that is correlated with  $\phi_{\text{halo}}$ . This means that the interval during which both terms are important is short and, to first approximation, this correction can be ignored.

For the purpose of simplifying our numerical analysis, the total halo contribution in Eq. (12), including energy deposition efficiency effects, can be approximated by

$$g_{\text{p}}(z, m_\chi, v_{\text{ref}}) \simeq f_{\text{s}}(z, m_\chi) G_{\text{p}}(z, v_{\text{ref}}) \quad (23)$$

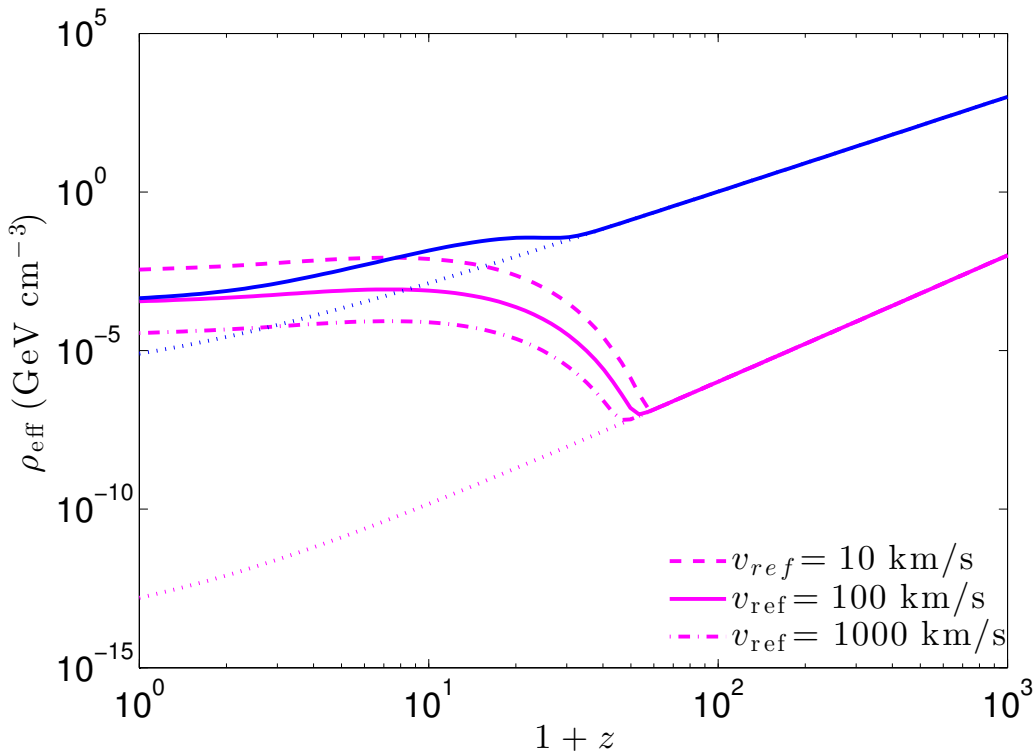


FIG. 2. Effective DM density  $\rho_{\text{eff}}$  as defined in Eqs. (19) (blue upper curves:  $s$ -wave annihilation) and (20) (magenta lower curves:  $p$ -wave annihilation). In each case, the monotonically increasing dotted line is the smooth DM background contribution, and the bump at low  $z$  represents the halo contribution. The  $p$ -wave case is given for three values of  $v_{\text{ref}}$  and we have chosen a redshift of thermal decoupling  $z_{\text{KD}} = 10^8$ . This figure is for illustration and does not represent a particular model of kinetic decoupling.

and

$$G_{\text{p}}(z, v_{\text{ref}}) = \left( \frac{100 \text{ km/s}}{v_{\text{ref}}} \right)^2 G_{\text{p}}(z, 100 \text{ km/s}). \quad (24)$$

In Appendix B we provide the steps to compute the complete halo contribution, along with a fitting formula that approximates this quantity, which we use to compute the exclusion regions presented in Section III. Finally, we note that this approach does not include the additional effect of substructure, which could serve to boost the late-time signal from annihilating DM – and thus tighten constraints – even further.

Since the background contribution to ionization by  $p$ -wave DM annihilations is highly suppressed, the halo contribution, which begins with structure formation around  $z \sim 50$ , would dominate any observable effects. In the right-hand panel of Fig. 1, we show the free electron fraction  $x_e(z)$  as a function of the redshift with and without DM contributions. Again, the light blue band corresponds to Planck results in the absence of a component from DM annihilation. The three other curves show  $x_e(z)$  due to a 5 GeV DM candidate which fully annihilates into  $e^+e^-$  through a  $p$ -wave suppressed process. We simultaneously consider reionization by stars at  $z_{\text{reio}} = 7$ , which cannot account for Planck results by itself. In Fig. 1 we see that, for instance, if  $\sigma v_{\text{ref}} \sim 10^{-22} \text{ cm}^3$ , a mixed DM-stars reionization scenario matches CMB data (although a larger  $z_{\text{reio}} \sim 9$  is actually necessary to get a good agreement with CMB data with such a cross section).

Parameter	Prior
$\Omega_{b,0}h^2$	0.005 $\rightarrow$ 0.1
$\Omega_{\text{DM},0}h^2$	0.01 $\rightarrow$ 0.99
$\Theta_s$	0.5 $\rightarrow$ 10
$z_{\text{reio}}$	7 $\rightarrow$ 12
$n_s$	0.5 $\rightarrow$ 1.5
$\ln(10^{10}A_s)$	2.7 $\rightarrow$ 4
$\tau_\chi/(10^{24}\text{s})$	$10^{-2} \rightarrow 10^5$
$\sigma v_{\text{ref}}/(3 \times 10^{-26}\text{cm}^3/\text{s})$	$10^0 \rightarrow 10^{12}$

TABLE I. Priors on the cosmological parameters used in this work, including the DM lifetime and the p-wave annihilation cross section.

### III. RESULTS

In this section we present the results of our Markov Chain Monte Carlo (MCMC) studies for both DM decays and p-wave annihilations. For each DM mass  $m_\chi$ , the parameters considered in these two MCMC analyses are

$$\{\omega_b, \omega_{\text{DM}}, \Theta_s, z_{\text{reio}}, n_s, \log[10^{10}A_s]\} + \tau_\chi \text{ (decays) or } \sigma v_{\text{ref}} \text{ (p-wave annihilations)}, \quad (25)$$

where  $\omega_b \equiv \Omega_{b,0}h^2$  and  $\omega_{\text{DM}} \equiv \Omega_{\text{DM},0}h^2$  are the physical baryon and cold DM energy densities today,  $\Theta_s$  is the ratio between the sound horizon and the angular diameter distance at decoupling,  $z_{\text{reio}}$  is the reionization redshift,  $n_s$  is the scalar spectral index,  $A_s$  is the amplitude of the primordial spectrum, and  $\tau_\chi$  and  $\sigma v_{\text{ref}}$  are the DM lifetime and the p-wave cross section times the relative velocity (for a reference value  $v_{\text{ref}}$ ), respectively. We make use of the Boltzmann code CAMB [61] as well as the publicly available MCMC package `cosmomc` [80] with the recombination module `CosmoRec` [18, 55–60]. We show in Tab. I the flat priors on the above parameters.

We have performed an analysis with the WMAP9 data [40] (temperature and polarization) combined with SPT data [41, 42], which includes nuisance parameters related to the Sunyaev–Zeldovich amplitude,  $A_{SZ}$ , to the amplitude of the clustered point source contribution  $A_C$ , and to the amplitude of the Poisson distributed point source contribution  $A_P$ . We have also separately included high multipole data from the ACT CMB experiment [43], obtaining very similar constraints to the case with SPT, which we do not show. In addition to CMB measurements, we include a prior on the Hubble constant  $H_0$  from the HST [44] and BAO measurements from a number of surveys [45–48]. Nevertheless, the addition of the former two external data sets does not significantly improve the results. We have also performed an analysis with the recent Planck CMB data [34], considering the high- $\ell$  TT likelihood with measurements up to  $\ell_{\text{max}} = 2500$ , combined with the low- $\ell$  TT likelihood, which accounts for measurements up to  $\ell = 49$  and the low- $\ell$  ( $\ell = 23$ ) TE, EE, BB likelihood [81] by including WMAP9 polarization measurements. We include the lensing likelihood as well as external data from HST and BAO measurements. High multipole information from both ACT and SPT experiments is also added, this time simultaneously, following the analyses presented by the Planck collaboration. All foreground parameters have been marginalized over as in Ref. [34].

Following previous works [16, 26, 33], we have also considered the IGM temperature as an additional constraint. Lyman- $\alpha$  observations indicate that the IGM temperature is of the order of a few times  $10^4$  K in the redshift interval  $2 < z < 4.5$  [49]. Thus, the total likelihood is supplemented by the temperature likelihood, by means of a half-gaussian distribution with a mean  $T_m = 11220$  K and a standard deviation  $\sigma_{T_m} = 8780$  K at a redshift  $z = 4.3$ . In other words, we only consider temperature bounds when the IGM temperature of a given model at  $z = 4.3$  is larger than  $T_m = 11220$  K.

In Fig. 3 we show the 95% CL limits on DM decays in the  $(m_\chi, \tau_\chi)$  plane for three different channels, which bracket the limits into other SM decay channels. Unlike what occurs in the case of s-wave DM annihilations, the measurement of the IGM temperature  $T_m$  contributes significantly to the bounds and further constrains DM energy injection due to the redshift dependence of DM decays, with late injection becoming increasingly important just as bounds from the IGM temperature start to be significant. The most stringent lower limit on the DM lifetime we obtain is  $\tau_\chi/f_{\text{eff,dec}}(m_\chi) \gtrsim 4 \times 10^{25}$  s. Let us mention that bounds from gamma-ray searches are at the level of  $\tau_\chi \gtrsim 10^{26} - 10^{27}$  s, depending on the target region and DM mass [82–86], and bounds from antiproton searches on hadronically decaying DM are slightly stronger [87, 88]. On the other hand, our limits are better than those from neutrino searches [89–91] for  $m_\chi \lesssim 100$  GeV. See Ref. [92] for a recent update (and a more complete list of references) on limits for unstable DM.

In Fig. 4 we depict the 95% CL limits in the  $(m_\chi, \sigma v_{\text{ref}})$  plane on p-wave DM annihilation cross sections for



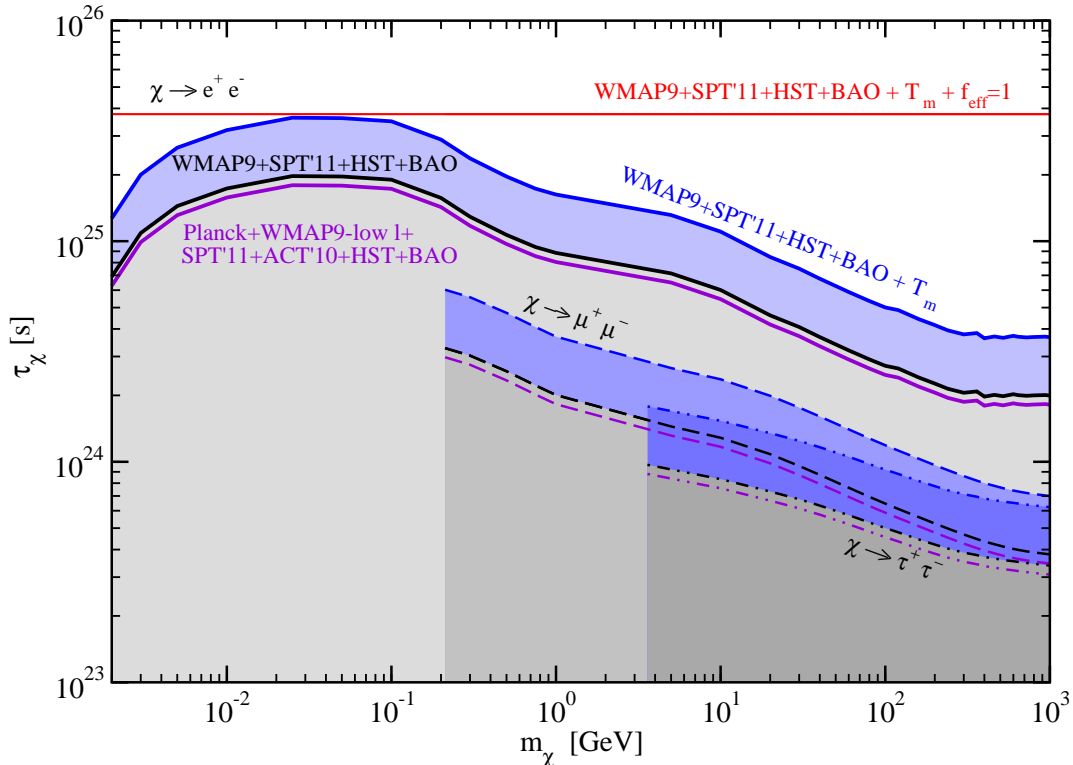


FIG. 3. Limits on the DM lifetime  $\tau_\chi$  at 95% CL. The upper red horizontal line assumes 100% energy deposition efficiency. Notice that Planck and WMAP9 constraints (combined with the external data sets) are very similar. Including the efficiency  $f_{\text{eff,dec}}(m_\chi)$  gives the weaker, colored constraints. We illustrate decays into  $e^+e^-$  (longest solid lines),  $\mu^+\mu^-$  (long dashed lines) and  $\tau^+\tau^-$  (short dashed-dotted lines). The different colors refer to the different data sets: black (blue) and violet refer to WMAP9 plus SPT'11 plus HST+BAO (plus also the prior on  $T_m$ ) and to Planck plus WMAP9 low- $l$  polarization measurements plus CMB high- $l$  (ACT'10 and SPT'11) plus HST+BAO data sets, respectively. Constraints on decays into two quarks or two weak gauge bosons lie between the  $e^+e^-$  and  $\tau^+\tau^-$  lines.

three different channels, which bracket the limits into other SM annihilation channels. To avoid a very busy plot, we only show the limits obtained with WMAP9+SPT'11+HST+BAO (black lines and grey regions) and those with Planck+WMAP9-low $l$ +ACT'10+SPT'11+HST+BAO+ $T_m$  (green lines and regions). As in the case of DM decays, the bounds from WMAP9 and Planck are very similar, and the principal source of improvement between the upper and lower limits is the addition of the prior on  $T_m$ . This indicates that measurements of the IGM temperature provide a powerful tool to constrain late-time energy injection mechanisms. In spite of this, the annihilation cross sections probed in Fig. 4 are still many orders of magnitude above the cross section required for thermal production ( $b \sim 2 \times 10^{-25} \text{ cm}^3/\text{s}$ ), making these exclusions specifically relevant for DM which was not produced via a standard chemical freeze-out. Nevertheless, we note that in the mass range studied here, these constraints are already stronger than the general bound from unitarity arguments, applied to p-wave dominated annihilation cross sections [93],

$$\sigma v \leq 1.3 \times 10^{-12} \text{ cm}^3/\text{s} \left( \frac{\text{GeV}}{m_\chi} \right)^2 \left( \frac{100 \text{ km/s}}{v_{\text{rms}}} \right). \quad (26)$$

Given that the dispersion velocity in halos is typically of order  $\mathcal{O}(100 \text{ km/s})$ , we have set  $v_{\text{ref}} = 100 \text{ km/s}$ , to facilitate comparison with bounds from indirect detection. As discussed above, these constraints come only from the halo contribution. Indeed, the  $(1+z)^8/(1+z_{\text{ref}})^2$  suppression to the annihilation rate of the homogeneous cosmological DM background means that its contribution is completely negligible as compared to the energy injected by annihilations in halos. This is indeed the opposite situation to what happens in the case of s-wave annihilations.

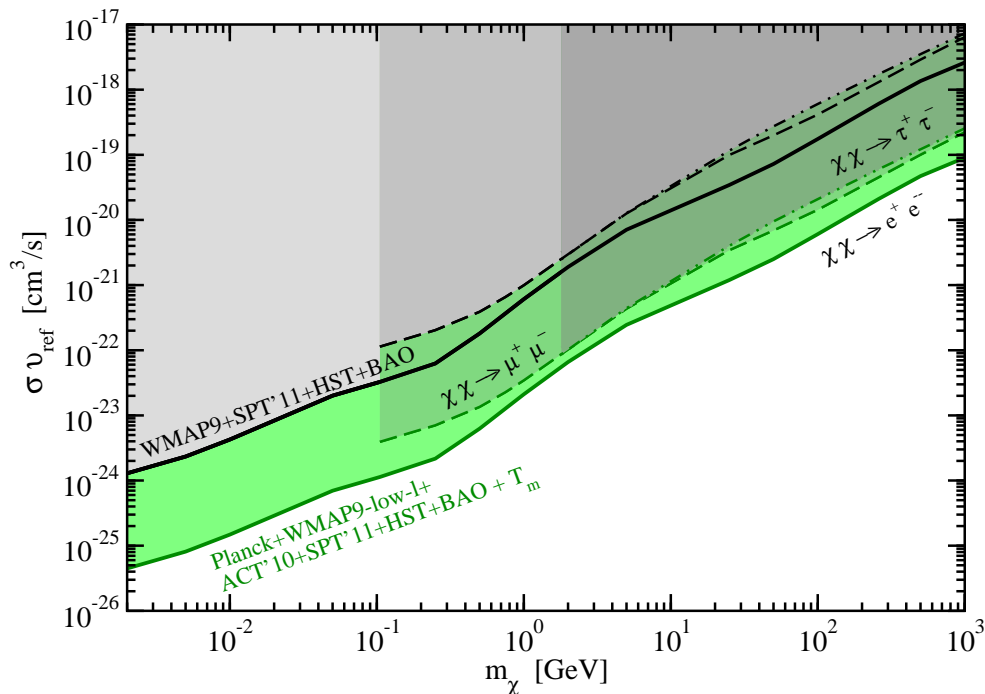


FIG. 4. Limits on the  $p$ -wave DM annihilation cross section  $\sigma v_{\text{ref}} = b v_{\text{ref}}^2$  with  $v_{\text{ref}} = 100$  km/s, at 95% CL. The grey regions represent the constraints from CMB measurements only (WMAP9+SPT'11) plus HST+BAO, whereas the green regions use Planck data, WMAP9 low- $\ell$  data, ACT'10+SPT'11, HST+BAO, as well as with a prior on the IGM temperature  $T_m$ . See the text for details. The different lines represent DM annihilations into  $e^+e^-$  (solid lines),  $\mu^+\mu^-$  (dashed lines) and  $\tau^+\tau^-$  (dashed-dotted lines). Constraints on annihilations into two quarks or two weak gauge bosons lie between the  $e^+e^-$  and  $\tau^+\tau^-$  lines. Note that the improvements on the bounds between the upper and lower curves are mainly driven by the inclusion of  $T_m$ , rather than Planck data. A very similar result to the lower curves is obtained when adding the  $T_m$  prior to the WMAP9+SPT'11+HST+BAO data sets.

#### IV. CONCLUSIONS

Energy injection into the IGM may have important effects on the temperature and polarization spectra of the CMB by modifying the ionization history of the Universe after recombination. If DM annihilates or decays into SM particles, the produced high-energy electrons and photons would provide an extra source of ionization and heating that would alter the CMB. In recent years, many analyses have been performed to set constraints on the  $s$ -wave dominated DM annihilation cross section using CMB data [1–23, 25–34]. Indeed, these limits are very stringent for candidates with masses below a few tens of GeV (see Refs. [33, 34] for the latest results using WMAP9 and Planck data). Likewise, late-time energy injection would raise the temperature of the IGM and this effect can be used to further constrain the maximum allowed amount of injected energy at low redshifts [16, 26, 33].

In this work, we have examined two mechanisms by which DM would release energy into the IGM with important effects at late times: DM decays and  $p$ -wave annihilations. In order to set constraints, we have used the latest available CMB data: the recent Planck data [34], WMAP9 polarization and temperature data [40] and the high-multipole SPT [41, 42] and ACT [43] data. We have also added a prior on  $H_0$  from the results of the HST [44] and from BAO observations [45–48]. Finally, we have also added a prior on the matter temperature obtained from Lyman- $\alpha$  observations at redshifts  $2 < z < 4.5$  [49]. Indeed, the latter prior tightens the bounds in a very significant way.

In Fig. 3 we show our results for DM decays which, using CMB data and adding the prior on  $T_m$ , represent a lower bound on the DM lifetime,  $\tau_\chi / f_{\text{eff,dec}}(m_\chi) \gtrsim 4 \times 10^{25}$  s. As decays occur increasingly with time (the DM lifetime is larger than the age of the Universe), low-multipole temperature and polarization measurements are the most sensitive

ones when using CMB data.

In Fig. 4 we depict the constraints we obtain for p-wave DM annihilation cross sections. Like for decays, the main effects occur at low redshifts, although for a different reason. As DM particles begin clustering into halos, their contribution becomes more important than the background one. In the case of velocity-independent annihilation cross sections, the overall contribution from halos is smaller than that from the smooth DM background at early times, close to recombination, so the limits are set by the effects caused by the latter. However, for velocity-dependent annihilation cross sections, there is a further enhancement in the contribution from halos (see Fig. 2) due to the much larger velocity of particles in halos as compared to that of the background DM. Hence, the contribution from halos could even dominate the overall energy injection and it is actually the source driving the best limits by several orders of magnitude.

Since the most important contribution to observable effects in either scenario comes from late-time effects, we have found that the current determination of the IGM temperature at  $z \sim 4$  solidly strengthens the respective constraints on the decay rate and cross section. While the upcoming release of Planck polarization data should improve the CMB constraints, more accurate measurements of the IGM temperature would significantly improve constraints on energy injection after recombination from DM decays and p-wave annihilations.

## V. ACKNOWLEDGMENTS

We would like to thank Jens Chluba for help with the CosmoRec code. LLH is supported through an ‘‘FWO-Vlaanderen’’ post-doctoral fellowship project number 1271513. LLH also recognizes partial support from the Belgian Federal Science Policy Office through the Interuniversity Attraction Pole P7/37 and from the Strategic Research Program ‘‘High-Energy Physics’’ of the Vrije Universiteit Brussel. OM is supported by the Consolider Ingenio project CSD2007-00060, by PROMETEO/2009/116, by the Spanish Grant FPA2011-29678 of the MINECO. SPR is supported by FPA2011-23596 of the MINECO. ACV acknowledges support from FQRNT and European contracts FP7-PEOPLE-2011-ITN. OM, SPR and ACV are also supported by PITN-GA-2011-289442-INVISIBLES. OM gratefully acknowledges the hospitality and financial support of the CERN Theoretical Physics Division.

### Appendix A: Energy deposition efficiency for decaying DM

Tab. II presents the values of  $f_{\text{eff,dec}}(m_\chi)$  for the three decay channels and for the specific values of the DM mass  $m_\chi$  that were used in our MCMC analyses.

### Appendix B: Detailed calculation of the halo function $g_p(z, m_\chi v_{\text{ref}})$

The energy injection via DM annihilations taking place in halos at a given redshift  $z$  is given by

$$\left( \frac{dE}{dV dt} \right)_{\text{halo, injected}} = \int dM \frac{dn(M, z)}{dM} \int_0^{r_\Delta} dr 4\pi r^2 \frac{\langle \sigma v \rangle}{m_\chi} \rho_{\text{halo}}^2(r), \quad (\text{B1})$$

where the first integral represents the sum of the contributions from all halos and the second integral is the contribution from a single halo and  $\rho_{\text{halo}}(r)$  is the density profile. In Eq. (B1), we use the physical halo mass function  $dn(M, z)/dM$  which is related to the comoving one by  $dn(M, z)/dM = (1+z)^3 dn_{\text{comov}}(M, z)/dM$ . We incorporate this contribution in the total deposited energy in the IGM of Eq. (12) in the case of p-wave annihilation making use of

$$g_p(z, m_\chi, v_{\text{ref}}) = \frac{H(z)}{(1+z)^3 \sum_i \int E \frac{dN}{dE} dE} \sum_i \int dz' \frac{(1+z')^2}{H(z')} G_p(z', v_{\text{ref}}) \int T_i(z', z, E) E \frac{dN}{dE} dE, \quad (\text{B2})$$

that depends on the dimensionless function  $G_p(z, v_{\text{ref}})$ , defined in Eq. (22) and which we reproduce here,

$$G_p(z, v_{\text{ref}}) \equiv \frac{1}{(\Omega_{\text{DM},0} \rho_{c,0})^2} \frac{1}{(1+z)^6} \int dM \frac{dn(M, z)}{dM} \int_0^{r_\Delta} dr 4\pi r^2 \frac{\langle v^2(r) \rangle}{v_{\text{ref}}^2} \rho_{\text{halo}}^2(r). \quad (\text{B3})$$

The squared dispersion velocity of DM particles in the halo is  $\langle v^2(r) \rangle$ , which depends on the DM location inside the halo is due to the p-wave dependence of the annihilation cross section parametrized as  $\langle \sigma v \rangle = \sigma v_{\text{ref}} \frac{\langle v^2(r) \rangle}{v_{\text{ref}}^2}$ . As in

$m_\chi(\text{GeV})$	$e$ channel	$\mu$ channel	$\tau$ channel
0.002	0.33695	–	–
0.003	0.53146	–	–
0.005	0.70445	–	–
0.01	0.8469	–	–
0.025	0.96321	–	–
0.05	0.95929	–	–
0.1	0.92764	–	–
0.2	0.76683	1.5997*	–
0.3	0.63069	0.14799	–
0.5	0.5216	0.12527	–
0.75	0.45929	0.10747	–
1	0.43219	0.096771	–
5	0.3488	0.068654	0.0473**
10	0.29343	0.060441	0.039151
20	0.22504	0.050569	0.03421
30	0.19927	0.044771	0.031473
40	0.17951	0.040639	0.029407
60	0.15616	0.035291	0.026516
80	0.14221	0.031964	0.024513
100	0.13295	0.029716	0.023068
120	0.12932	0.02817	0.022004
160	0.11764	0.025714	0.020352
200	0.11052	0.023996	0.019219
240	0.10463	0.022648	0.01838
300	0.10038	0.021215	0.017545
360	0.10176	0.020275	0.017039
400	0.09641	0.019604	0.016679
460	0.098201	0.019057	0.016396
520	0.096794	0.018515	0.016112
600	0.098876	0.018084	0.015889
640	0.097941	0.017868	0.01577
720	0.097191	0.017524	0.015571
800	0.097653	0.017301	0.015427
940	0.098035	0.017017	0.015224
1000	0.097368	0.016897	0.015133

TABLE II. Values of the energy deposition function  $f_{\text{eff,dec}}(m_\chi)$ , Eq. (11) for DM decays, for each of the three channels considered in this work. (\*evaluated at  $m_\chi = 212$  MeV; \*\*evaluated at  $m_\chi = 3.6$  GeV). Values represented by a dash (–) are below the threshold mass  $2m_\ell$  to produce the final state particle  $\ell$ . Refs. [50, 51] only provide the spectra for DM masses above 10 GeV, so for decays into  $\tau^+\tau^-$  the values of  $f_{\text{eff,dec}}(m_\chi)$  are obtained via extrapolation for  $m_\chi < 10$  GeV.

Ref. [33], where we refer the reader for further details, we have used the results from Ref. [77] for the halo mass function and from Ref. [78] for the halo mass–concentration relation and have assumed an NFW DM density profile [79] for each individual halo,

$$\rho_{\text{halo}}(r) = \rho_s \frac{4}{(r/r_s)(1+r/r_s)^2}, \quad (\text{B4})$$

where  $r_s$  is the scale radius and  $\rho_s$  the density at that radial distance.

In order to compute the annihilation rates in halos we assume that halo formation is adiabatic, *i.e.*, that particles remain thermal as they contract and have a Maxwell–Boltzmann velocity distribution

$$f(v, \Sigma) = \frac{4\pi}{(2\pi\Sigma^2)^{3/2}} v^2 \exp\left(-\frac{1}{2}\frac{v^2}{\Sigma^2}\right), \quad (\text{B5})$$

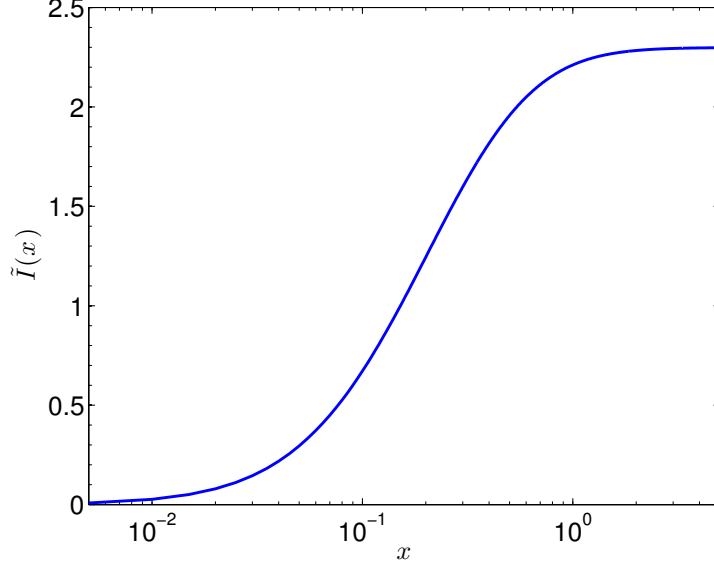


FIG. 5. The integral  $\tilde{I}(x)$  of Eq. (B13).

where  $\Sigma$  is the one-dimensional velocity dispersion (we use the notation  $\Sigma$  to avoid confusion with  $\sigma$ , the cross section). The squared velocity dispersion is then

$$\langle v^2(r) \rangle = 3\Sigma^2(r). \quad (\text{B6})$$

If we assume hydrostatic equilibrium, the velocity dispersion can be found by integrating the Jeans equation

$$\frac{d(\rho\Sigma^2)}{dr} = -\rho \frac{GM(< r)}{r^2}. \quad (\text{B7})$$

This can be done analytically with an NFW profile. The resulting distribution of the velocity dispersion is

$$\begin{aligned} \Sigma^2(x) = & \frac{8\pi G\rho_s r_s^2}{x} \left[ 6x^2(x+1)^2 \text{Li}_2(-x) + (x+1) \left\{ 3(x+1)x^2 \ln^2(x+1) \right. \right. \\ & + (x+1)x^2 \left( 6 \ln\left(\frac{1}{x} + 1\right) + 5 \ln(x) \right) - (x(x(5x+11)+3) - 1) \ln(x+1) \left. \right\} \\ & \left. + x \left( x \left( \pi^2(x+1)^2 - 7x - 9 \right) - 1 \right) \right], \end{aligned} \quad (\text{B8})$$

where  $x \equiv r/r_s$  and  $\text{Li}_2(x)$  is the dilogarithm function, the  $n = 2$  case of the polylogarithm

$$\text{Li}_n(z) \equiv \frac{1}{\Gamma(n)} \int_0^\infty \frac{t^{n-1}}{\frac{e^t}{z} - 1} dt. \quad (\text{B9})$$

We have checked that the assumption in Eq. (B8) is in reasonable agreement with the results of the N-body simulation Via Lactea II [94].

With these ingredients and the concentration parameter defined as  $c_\Delta = r_\Delta/r_s$ , we can rewrite Eq. (B3) as

$$G_p(z, v_{\text{ref}}) \equiv \frac{8\pi G r_s^5 \rho_s^3}{(\Omega_{\text{DM}} \rho_c)^2} \frac{1}{(1+z)^6} \int dM \frac{dn(M, z)}{dM} 4\pi r^2 \tilde{I}(c_\Delta), \quad (\text{B10})$$

where we have defined the dimensionless integral

$$\tilde{I}(x) \equiv \int_0^x z^2 \tilde{\rho}^2(z) 3\tilde{\Sigma}^2(z) dz = \frac{1}{8\pi G r_s^5 \rho_s^3} \int_0^{r_\Delta} dr r^2 \rho_{\text{halo}}^2(r) \langle v^2(r) \rangle, \quad (\text{B11})$$

$m_\chi$ (GeV)	$e$ channel	$\mu$ channel	$\tau$ channel
0.002	12.6886	–	–
0.005	17.5236	–	–
0.01	19.2091	–	–
0.05	20.3546	–	–
0.105	26.3105	7.572	–
0.25	32.6992	10.073	–
0.5	22.6522	10.519	–
0.75	16.7136	9.3534	–
1	13.4614	8.2243	–
1.8	9.2348	5.8579	5.9211
5	5.7843	3.2559	3.2101
25	5.9451	2.0627	1.7675
50	5.664	2.0536	1.4973
100	4.6891	1.976	1.3591
260	3.506	1.6286	1.2262
500	3.0174	1.4131	1.1676
1000	3.1416	1.2796	1.1168

TABLE III. Value of  $\gamma_{\text{p}(i,m_\chi)}$  to be inserted into Eq. (B15) to approximate  $g_{\text{p}}(z, m_\chi, v_{\text{ref}})$ . Refs. [50, 51] only provide the spectra for DM masses above 5 GeV, so for annihilations into  $\tau^+\tau^-$  the value of  $\gamma_{\text{p}(i,m_\chi)}$  is obtained via extrapolation for  $m_\chi = 1.8$  GeV.

with

$$\tilde{\rho} = \frac{\rho}{\rho_s} \quad ; \quad \tilde{\Sigma}^2 = \frac{\Sigma^2}{8\pi G\rho_s r_s^2}. \quad (\text{B12})$$

Thus, Eq. (B11) is explicitly given by

$$\begin{aligned} \tilde{I}(x) = & -16 \left[ 12\text{Li}_2 \left( -\frac{1}{x} \right) + 36\text{Li}_3(x+1) - \frac{18\text{Li}_2(x+1)(2x + (x+1)\ln(x+1) + 1)}{x+1} \right. \\ & + \frac{3x(6x^2 - 3x + 2\pi^2(x+1)^2 - 21)}{(x+1)^3} - \frac{35}{(x+1)^3} - \frac{9(-3x-2)\ln^2(x+1)}{x+1} \\ & + 3(\ln(x) - \ln(x+1))^3 + 9\ln(x+1)(\ln(x) - \ln(x+1))^2 + \frac{9\ln(x+1)}{(x+1)^3} \\ & - \frac{3(\pi^2(x+1)^3 - x(2x(5x+11) + 15) + (x+1)^3\ln(x) + 6(2x+1)(x+1)^2\ln(-x))\ln(x+1)}{(x+1)^3} \\ & - \frac{3(\ln(x+1) - \ln(x))((9 + \pi^2)x - 4(x+1)\ln(x) + 6(x+1)\ln(x+1) + \pi^2 + 15)}{x+1} \\ & \left. - \frac{3\ln(x)((10 + \pi^2)x + (x+1)\ln(x)(\ln(x) + 2) + \pi^2 + 15)}{x+1} - 36\zeta(3) + 5\pi^2 + 35 \right]. \quad (\text{B13}) \end{aligned}$$

For  $z > 0$ ,  $\ln(-z)$  and  $\text{Li}_n(z)$  are complex. Taking consistent branch cuts, and noting that

$$\text{Im}\{\text{Li}_n(z + i\epsilon)\} = \frac{\pi \ln^{n-1}(z)}{\Gamma(n)}, \quad (\text{B14})$$

one can see that the imaginary parts of Eq. (B13) cancel, leaving a real expression. This expression is plotted in Fig. 5.

For relevant values of  $z \lesssim 50$ , we obtain the fit

$$g_{\text{p}}(z, m_\chi, 100 \text{ km/s}) \simeq f_s(z, m_\chi)G_{\text{p}}(z, 100 \text{ km/s}) \simeq \gamma_{\text{p}(i,m_\chi)}\Gamma_{\text{p}}(z, 100 \text{ km/s}), \quad (\text{B15})$$

where  $\gamma_{\text{p}(i,m_\chi)}$  depends on both the annihilation channel ( $i = \{e, \mu, \tau\}$ ) and on the DM mass  $m_\chi$ , see Tab. III. The function  $\Gamma_{\text{p}}(z, 100 \text{ km/s})$  is given by

$$\ln \Gamma_{\text{p}}(z, 100 \text{ km/s}) = a_3(1+z)^3 + a_2(1+z)^2 + a_1(1+z) + a_0 \quad (\text{B16})$$

with

$$a_3 = -7.379 \times 10^{-5}; \quad a_2 = -0.004499; \quad a_1 = -0.7012; \quad a_0 = 4.2. \quad (\text{B17})$$

Finally, we have

$$g_p(z, m_\chi, v_{\text{ref}}) = \left( \frac{100 \text{ km/s}}{v_{\text{ref}}} \right)^2 g_p(z, m_\chi, 100 \text{ km/s}). \quad (\text{B18})$$

- [1] X.-L. Chen and M. Kamionkowski, “Particle decays during the cosmic dark ages,” *Phys.Rev.* **D70** (2004) 043502, [arXiv:astro-ph/0310473](#) [[astro-ph](#)].
- [2] S. H. Hansen and Z. Haiman, “Do we need stars to reionize the universe at high redshifts? Early reionization by decaying heavy sterile neutrinos,” *Astrophys.J.* **600** (2004) 26–31, [arXiv:astro-ph/0305126](#) [[astro-ph](#)].
- [3] E. Pierpaoli, “Decaying particles and the reionization history of the universe,” *Phys.Rev.Lett.* **92** (2004) 031301, [arXiv:astro-ph/0310375](#) [[astro-ph](#)].
- [4] N. Padmanabhan and D. P. Finkbeiner, “Detecting dark matter annihilation with CMB polarization: Signatures and experimental prospects,” *Phys.Rev.* **D72** (2005) 023508, [arXiv:astro-ph/0503486](#) [[astro-ph](#)].
- [5] M. Mapelli, A. Ferrara, and E. Pierpaoli, “Impact of dark matter decays and annihilations on reionization,” *Mon.Not.Roy.Astron.Soc.* **369** (2006) 1719–1724, [arXiv:astro-ph/0603237](#) [[astro-ph](#)].
- [6] L. Zhang, X.-L. Chen, Y.-A. Lei, and Z.-G. Si, “The impacts of dark matter particle annihilation on recombination and the anisotropies of the cosmic microwave background,” *Phys.Rev.* **D74** (2006) 103519, [arXiv:astro-ph/0603425](#) [[astro-ph](#)].
- [7] E. Ripamonti, M. Mapelli, and A. Ferrara, “Intergalactic medium heating by dark matter,” *Mon.Not.Roy.Astron.Soc.* **374** (2007) 1067–1077, [arXiv:astro-ph/0606482](#) [[astro-ph](#)].
- [8] L. Zhang, X. Chen, M. Kamionkowski, Z.-g. Si, and Z. Zheng, “Constraints on radiative dark-matter decay from the cosmic microwave background,” *Phys.Rev.* **D76** (2007) 061301, [arXiv:0704.2444](#) [[astro-ph](#)].
- [9] L. Chuzhoy, “Impact of Dark Matter Annihilation on the High-Redshift Intergalactic Medium,” *Astrophys.J.* **679** (2008) L65–L68, [arXiv:0710.1856](#) [[astro-ph](#)].
- [10] D. P. Finkbeiner, N. Padmanabhan, and N. Weiner, “CMB and 21-cm Signals for Dark Matter with a Long-Lived Excited State,” *Phys.Rev.* **D78** (2008) 063530, [arXiv:0805.3531](#) [[astro-ph](#)].
- [11] A. Natarajan and D. J. Schwarz, “The effect of early dark matter halos on reionization,” *Phys.Rev.* **D78** (2008) 103524, [arXiv:0805.3945](#) [[astro-ph](#)].
- [12] A. Natarajan and D. J. Schwarz, “Dark matter annihilation and its effect on CMB and Hydrogen 21 cm observations,” *Phys.Rev.* **D80** (2009) 043529, [arXiv:0903.4485](#) [[astro-ph.CO](#)].
- [13] A. V. Belikov and D. Hooper, “How Dark Matter Reionized The Universe,” *Phys.Rev.* **D80** (2009) 035007, [arXiv:0904.1210](#) [[hep-ph](#)].
- [14] S. Galli, F. Iocco, G. Bertone, and A. Melchiorri, “CMB constraints on Dark Matter models with large annihilation cross-section,” *Phys.Rev.* **D80** (2009) 023505, [arXiv:0905.0003](#) [[astro-ph.CO](#)].
- [15] T. R. Slatyer, N. Padmanabhan, and D. P. Finkbeiner, “CMB Constraints on WIMP Annihilation: Energy Absorption During the Recombination Epoch,” *Phys.Rev.* **D80** (2009) 043526, [arXiv:0906.1197](#) [[astro-ph.CO](#)].
- [16] M. Cirelli, F. Iocco, and P. Panci, “Constraints on Dark Matter annihilations from reionization and heating of the intergalactic gas,” *JCAP* **0910** (2009) 009, [arXiv:0907.0719](#) [[astro-ph.CO](#)].
- [17] T. Kanzaki, M. Kawasaki, and K. Nakayama, “Effects of Dark Matter Annihilation on the Cosmic Microwave Background,” *Prog.Theor.Phys.* **123** (2010) 853–865, [arXiv:0907.3985](#) [[astro-ph.CO](#)].
- [18] J. Chluba, “Could the Cosmological Recombination Spectrum Help Us Understand Annihilating Dark Matter?,” *Mon.Not.Roy.Astron.Soc.* **402** (2010) 1195–1207, [arXiv:0910.3663](#) [[astro-ph.CO](#)].
- [19] M. Valdes, C. Evoli, and A. Ferrara, “Particle energy cascade in the Intergalactic Medium,” *Mon.Not.Roy.Astron.Soc.* **404** (2010) 1569–1582, [arXiv:0911.1125](#) [[astro-ph.CO](#)].
- [20] A. Natarajan and D. J. Schwarz, “Distinguishing standard reionization from dark matter models,” *Phys.Rev.* **D81** (2010) 123510, [arXiv:1002.4405](#) [[astro-ph.CO](#)].
- [21] G. Hutsi, J. Chluba, A. Hektor, and M. Raidal, “WMAP7 and future CMB constraints on annihilating dark matter: implications on GeV-scale WIMPs,” *Astron.Astrophys.* **535** (2011) A26, [arXiv:1103.2766](#) [[astro-ph.CO](#)].
- [22] S. Galli, F. Iocco, G. Bertone, and A. Melchiorri, “Updated CMB constraints on Dark Matter annihilation cross-sections,” *Phys.Rev.* **D84** (2011) 027302, [arXiv:1106.1528](#) [[astro-ph.CO](#)].
- [23] D. P. Finkbeiner, S. Galli, T. Lin, and T. R. Slatyer, “Searching for Dark Matter in the CMB: A Compact Parameterization of Energy Injection from New Physics,” *Phys.Rev.* **D85** (2012) 043522, [arXiv:1109.6322](#) [[astro-ph.CO](#)].
- [24] A. Natarajan, “A closer look at CMB constraints on WIMP dark matter,” *Phys.Rev.* **D85** (2012) 083517, [arXiv:1201.3939](#) [[astro-ph.CO](#)].
- [25] C. Evoli, M. Valdes, A. Ferrara, and N. Yoshida, “Energy deposition by weakly interacting massive particles: a comprehensive study,” *Mon.Not.Roy.Astron.Soc.* **422** (2012) 420–433.

- [26] G. Giesen, J. Lesgourgues, B. Audren, and Y. Ali-Haïmoud, “CMB photons shedding light on dark matter,” *JCAP* **1212** (2012) 008, [arXiv:1209.0247 \[astro-ph.CO\]](#).
- [27] C. Evoli, S. Pandolfi, and A. Ferrara, “CMB constraints on light dark matter candidates,” *Mon.Not.Roy.Astron.Soc.* **433** (2013) 1736–1744, [arXiv:1210.6845 \[astro-ph.CO\]](#).
- [28] T. R. Slatyer, “Energy Injection And Absorption In The Cosmic Dark Ages,” *Phys.Rev.* **D87** (2012) 123513, [arXiv:1211.0283 \[astro-ph.CO\]](#).
- [29] A. R. Frey and N. B. Reid, “Cosmic Microwave Background Constraints on Dark Matter Models of the Galactic Center 511 keV Signal,” *Phys.Rev.* **D87** (2013) 103508, [arXiv:1301.0819 \[hep-ph\]](#).
- [30] J. M. Cline and P. Scott, “Dark Matter CMB Constraints and Likelihoods for Poor Particle Physicists,” *JCAP* **1303** (2013) 044, [arXiv:1301.5908 \[astro-ph.CO\]](#).
- [31] C. Weniger, P. D. Serpico, F. Iocco, and G. Bertone, “CMB bounds on dark matter annihilation: Nucleon energy-losses after recombination,” *Phys. Rev. D* **87**, **123008** (2013), [arXiv:1303.0942 \[astro-ph.CO\]](#).
- [32] C. Dvorkin, K. Blum, and M. Zaldarriaga, “Perturbed Recombination from Dark Matter Annihilation,” *Phys. Rev. D.* **87** (2013) 103522, [arXiv:1302.4753 \[astro-ph.CO\]](#).
- [33] L. Lopez-Honorez, O. Mena, S. Palomares-Ruiz, and A. C. Vincent, “Constraints on dark matter annihilation from CMB observations before Planck,” *JCAP* **1307** (2013) 046, [arXiv:1303.5094 \[astro-ph.CO\]](#).
- [34] **Planck** Collaboration, P. Ade *et al.*, “Planck 2013 results. XVI. Cosmological parameters,” [arXiv:1303.5076 \[astro-ph.CO\]](#).
- [35] M. S. Madhavacheril, N. Sehgal, and T. R. Slatyer, “Current Dark Matter Annihilation Constraints from CMB and Low-Redshift Data,” [arXiv:1310.3815 \[astro-ph.CO\]](#).
- [36] M. Srednicki, R. Watkins, and K. A. Olive, “Calculations of Relic Densities in the Early Universe,” *Nucl.Phys.* **B310** (1988) 693.
- [37] P. Gondolo and G. Gelmini, “Cosmic abundances of stable particles: Improved analysis,” *Nucl.Phys.* **B360** (1991) 145–179.
- [38] K. Griest and D. Seckel, “Three exceptions in the calculation of relic abundances,” *Phys.Rev.* **D43** (1991) 3191–3203.
- [39] G. Steigman, B. Dasgupta, and J. F. Beacom, “Precise Relic WIMP Abundance and its Impact on Searches for Dark Matter Annihilation,” *Phys.Rev.* **D86** (2012) 023506, [arXiv:1204.3622 \[hep-ph\]](#).
- [40] **WMAP** Collaboration, G. Hinshaw *et al.*, “Nine-Year Wilkinson Microwave Anisotropy Probe (WMAP) Observations: Cosmological Parameter Results,” *Astrophys.J.Suppl.* **208** (2013) 19, [arXiv:1212.5226 \[astro-ph.CO\]](#).
- [41] **SPT** Collaboration, K. Story *et al.*, “A Measurement of the Cosmic Microwave Background Damping Tail from the 2500-square-degree SPT-SZ survey,” [arXiv:1210.7231 \[astro-ph.CO\]](#).
- [42] **SPT** Collaboration, Z. Hou *et al.*, “Constraints on Cosmology from the Cosmic Microwave Background Power Spectrum of the 2500-square degree SPT-SZ Survey,” [arXiv:1212.6267 \[astro-ph.CO\]](#).
- [43] **Atacama Cosmology Telescope** Collaboration, J. L. Sievers *et al.*, “The Atacama Cosmology Telescope: Cosmological parameters from three seasons of data,” *JCAP* **1310** (2013) 060, [arXiv:1301.0824 \[astro-ph.CO\]](#).
- [44] A. G. Riess *et al.*, “A 3% Solution: Determination of the Hubble Constant with the Hubble Space Telescope and Wide Field Camera 3,” *Astrophys.J.* **730** (2011) 119, [arXiv:1103.2976 \[astro-ph.CO\]](#).
- [45] **BOSS** Collaboration, L. Anderson *et al.*, “The clustering of galaxies in the SDSS-III Baryon Oscillation Spectroscopic Survey: Baryon Acoustic Oscillations in the Data Release 9 Spectroscopic Galaxy Sample,” *Mon.Not.Roy.Astron.Soc.* **427** (2013) 3435–3467, [arXiv:1203.6594 \[astro-ph.CO\]](#).
- [46] N. Padmanabhan, X. Xu, D. J. Eisenstein, R. Scalzo, A. J. Cuesta, K. T. Mehta, and E. Kazin, “A 2% Distance to  $z = 0.35$  by Reconstructing Baryon Acoustic Oscillations - I : Methods and Application to the Sloan Digital Sky Survey,” *Mon.Not.Roy.Astron.Soc.* **427** (2012) 2132–2145, [arXiv:1202.0090 \[astro-ph.CO\]](#).
- [47] F. Beutler *et al.*, “The 6dF Galaxy Survey: Baryon Acoustic Oscillations and the Local Hubble Constant,” *Mon.Not.Roy.Astron.Soc.* **416** (2011) 3017–3032, [arXiv:1106.3366 \[astro-ph.CO\]](#).
- [48] C. Blake *et al.*, “The WiggleZ Dark Energy Survey: mapping the distance-redshift relation with baryon acoustic oscillations,” *Mon.Not.Roy.Astron.Soc.* **418** (2011) 1707–1724, [arXiv:1108.2635 \[astro-ph.CO\]](#).
- [49] J. Schaye, T. Theuns, M. Rauch, G. Efstathiou, and W. L. Sargent, “The Thermal history of the intergalactic medium,” *Mon.Not.Roy.Astron.Soc.* **318** (2000) 817, [arXiv:astro-ph/9912432 \[astro-ph\]](#).
- [50] P. Ciafaloni, D. Comelli, A. Riotto, F. Sala, A. Strumia, *et al.*, “Weak Corrections are Relevant for Dark Matter Indirect Detection,” *JCAP* **1103** (2011) 019, [arXiv:1009.0224 \[hep-ph\]](#).
- [51] M. Cirelli, G. Corcella, A. Hektor, G. Hutsi, M. Kadastik, *et al.*, “PPPC 4 DM ID: A Poor Particle Physicist Cookbook for Dark Matter Indirect Detection,” *JCAP* **1103** (2011) 051, [arXiv:1012.4515 \[hep-ph\]](#).
- [52] S. Galli, T. R. Slatyer, M. Valdes, and F. Iocco, “Systematic Uncertainties In Constraining Dark Matter Annihilation From The Cosmic Microwave Background,” [arXiv:1306.0563 \[astro-ph.CO\]](#).
- [53] A. Doroshkevich and P. Naselsky, “Ionization history of the universe as a test for superheavy dark matter particles,” *Phys.Rev.* **D65** (2002) 123517, [arXiv:astro-ph/0201212 \[astro-ph\]](#).
- [54] R. Bean, A. Melchiorri, and J. Silk, “Recombining WMAP: Constraints on ionizing and resonance radiation at recombination,” *Phys.Rev.* **D68** (2003) 083501, [arXiv:astro-ph/0306357 \[astro-ph\]](#).
- [55] J. Chluba and R. Thomas, “Towards a complete treatment of the cosmological recombination problem,” *Mon.Not.Roy.Astron.Soc.* **412** (2011) 748–764, [arXiv:1010.3631 \[astro-ph.CO\]](#).
- [56] Y. Ali-Haïmoud and C. M. Hirata, “Ultrafast effective multi-level atom method for primordial hydrogen recombination,” *Phys.Rev.* **D82** (2010) 063521, [arXiv:1006.1355 \[astro-ph.CO\]](#).
- [57] J. Chluba, G. Vasil, and L. Dursi, “Recombinations to the Rydberg States of Hydrogen and Their Effect During the



- Cosmological Recombination Epoch,” *Mon.Not.Roy.Astron.Soc.* **407** (2010) 599–612, [arXiv:1003.4928 \[astro-ph.CO\]](#).
- [58] D. Grin and C. M. Hirata, “Cosmological hydrogen recombination: The effect of extremely high- $n$  states,” *Phys.Rev.* **D81** (2010) 083005, [arXiv:0911.1359 \[astro-ph.CO\]](#).
- [59] E. R. Switzer and C. M. Hirata, “Primordial helium recombination. 3. Thomson scattering, isotope shifts, and cumulative results,” *Phys.Rev.* **D77** (2008) 083008, [arXiv:astro-ph/0702145 \[ASTRO-PH\]](#).
- [60] J. Rubino-Martin, J. Chluba, W. Fendt, and B. Wandelt, “Estimating the impact of recombination uncertainties on the cosmological parameter constraints from cosmic microwave background experiments,” *Mon.Not.Roy.Astron.Soc.* **403** (2010) 439–452, [arXiv:0910.4383 \[astro-ph.CO\]](#).
- [61] A. Lewis, A. Challinor, and A. Lasenby, “Efficient computation of CMB anisotropies in closed FRW models,” *Astrophys.J.* **538** (2000) 473–476, [arXiv:astro-ph/9911177 \[astro-ph\]](#).
- [62] C. Schmid, D. J. Schwarz, and P. Widerin, “Amplification of cosmological inhomogeneities from the QCD transition,” *Phys.Rev.* **D59** (1999) 043517, [arXiv:astro-ph/9807257 \[astro-ph\]](#).
- [63] K. Zybin, M. Vysotsky, and A. Gurevich, “The fluctuation spectrum cutoff in a neutralino dark matter scenario,” *Phys.Lett.* **A260** (1999) 262–268.
- [64] X.-l. Chen, M. Kamionkowski, and X.-m. Zhang, “Kinetic decoupling of neutralino dark matter,” *Phys.Rev.* **D64** (2001) 021302, [arXiv:astro-ph/0103452 \[astro-ph\]](#).
- [65] S. Hofmann, D. J. Schwarz, and H. Stoecker, “Damping scales of neutralino cold dark matter,” *Phys.Rev.* **D64** (2001) 083507, [arXiv:astro-ph/0104173 \[astro-ph\]](#).
- [66] V. Berezhinsky, V. Dokuchaev, and Y. Eroshenko, “Small - scale clumps in the galactic halo and dark matter annihilation,” *Phys.Rev.* **D68** (2003) 103003, [arXiv:astro-ph/0301551 \[astro-ph\]](#).
- [67] A. M. Green, S. Hofmann, and D. J. Schwarz, “The First wimpy halos,” *JCAP* **0508** (2005) 003, [arXiv:astro-ph/0503387 \[astro-ph\]](#).
- [68] A. Loeb and M. Zaldarriaga, “The Small-scale power spectrum of cold dark matter,” *Phys.Rev.* **D71** (2005) 103520, [arXiv:astro-ph/0504112 \[astro-ph\]](#).
- [69] S. Profumo, K. Sigurdson, and M. Kamionkowski, “What mass are the smallest protohalos?,” *Phys.Rev.Lett.* **97** (2006) 031301, [arXiv:astro-ph/0603373 \[astro-ph\]](#).
- [70] E. Bertschinger, “The Effects of Cold Dark Matter Decoupling and Pair Annihilation on Cosmological Perturbations,” *Phys.Rev.* **D74** (2006) 063509, [arXiv:astro-ph/0607319 \[astro-ph\]](#).
- [71] T. Bringmann and S. Hofmann, “Thermal decoupling of WIMPs from first principles,” *JCAP* **0407** (2007) 016, [arXiv:hep-ph/0612238 \[hep-ph\]](#).
- [72] T. Bringmann, “Particle Models and the Small-Scale Structure of Dark Matter,” *New J.Phys.* **11** (2009) 105027, [arXiv:0903.0189 \[astro-ph.CO\]](#).
- [73] J. M. Cornell and S. Profumo, “Earthly probes of the smallest dark matter halos,” *JCAP* **1206** (2012) 011, [arXiv:1203.1100 \[hep-ph\]](#).
- [74] P. Gondolo, J. Hisano, and K. Kadota, “The Effect of quark interactions on dark matter kinetic decoupling and the mass of the smallest dark halos,” *Phys.Rev.* **D86** (2012) 083523, [arXiv:1205.1914 \[hep-ph\]](#).
- [75] J. M. Cornell, S. Profumo, and W. Shepherd, “Kinetic Decoupling and Small-Scale Structure in Effective Theories of Dark Matter,” *Phys. Rev. D* **88**, **015027** (2013), [arXiv:1305.4676 \[hep-ph\]](#).
- [76] I. M. Shoemaker, “Constraints on Dark Matter Protohalos in Effective Theories and Neutrinophilic Dark Matter,” *Phys.Dark.Univ.* **2** no. 3, (2013) 157–162, [arXiv:1305.1936 \[hep-ph\]](#).
- [77] W. A. Watson, I. T. Iliev, A. D’Aloisio, A. Knebe, P. R. Shapiro, and G. Yepes, “The halo mass function through the cosmic ages,” *Mon.Not.Roy.Astron.Soc.* **433** (2013) 1230–1245, [arXiv:1212.0095 \[astro-ph.CO\]](#).
- [78] F. Prada, A. A. Klypin, A. J. Cuesta, J. E. Betancort-Rijo, and J. Primack, “Halo concentrations in the standard LCDM cosmology,” *Mon.Not.Roy.Astron.Soc.* **423** (2012) 3018–3030, [arXiv:1104.5130 \[astro-ph.CO\]](#).
- [79] J. F. Navarro, C. S. Frenk, and S. D. M. White, “The Structure of Cold Dark Matter Halos,” *Astrophys. J.* **462** (1996) 563, [arXiv:astro-ph/9508025](#).
- [80] A. Lewis and S. Bridle, “Cosmological parameters from CMB and other data: A Monte Carlo approach,” *Phys.Rev.* **D66** (2002) 103511, [arXiv:astro-ph/0205436 \[astro-ph\]](#).
- [81] **WMAP** Collaboration, C. Bennett *et al.*, “Nine-Year Wilkinson Microwave Anisotropy Probe (WMAP) Observations: Final Maps and Results,” *Astrophys.J.Suppl.* **208** (2013) 20, [arXiv:1212.5225 \[astro-ph.CO\]](#).
- [82] **Fermi-LAT** Collaboration, A. Abdo *et al.*, “Constraints on Cosmological Dark Matter Annihilation from the Fermi-LAT Isotropic Diffuse Gamma-Ray Measurement,” *JCAP* **1004** (2010) 014, [arXiv:1002.4415 \[astro-ph.CO\]](#).
- [83] L. Dugger, T. E. Jeltema, and S. Profumo, “Constraints on Decaying Dark Matter from Fermi Observations of Nearby Galaxies and Clusters,” *JCAP* **1012** (2010) 015, [arXiv:1009.5988 \[astro-ph.HE\]](#).
- [84] X. Huang, G. Vertongen, and C. Weniger, “Probing Dark Matter Decay and Annihilation with Fermi LAT Observations of Nearby Galaxy Clusters,” *JCAP* **1201** (2012) 042, [arXiv:1110.1529 \[hep-ph\]](#).
- [85] M. Cirelli, E. Moulín, P. Panci, P. D. Serpico, and A. Viana, “Gamma ray constraints on Decaying Dark Matter,” *Phys.Rev.* **D86** (2012) 083506, [arXiv:1205.5283 \[astro-ph.CO\]](#).
- [86] **Fermi-LAT** Collaboration, M. Ackermann *et al.*, “Constraints on the Galactic Halo Dark Matter from Fermi-LAT Diffuse Measurements,” *Astrophys.J.* **761** (2012) 91, [arXiv:1205.6474 \[astro-ph.CO\]](#).
- [87] M. Garny, A. Ibarra, and D. Tran, “Constraints on Hadronically Decaying Dark Matter,” *JCAP* **1208** (2012) 025, [arXiv:1205.6783 \[hep-ph\]](#).
- [88] T. Delahaye and M. Grefe, “Antiproton Limits on Decaying Gravitino Dark Matter,” [arXiv:1305.7183 \[hep-ph\]](#).
- [89] S. Palomares-Ruiz, “Model-Independent Bound on the Dark Matter Lifetime,” *Phys.Lett.* **B665** (2008) 50–53,

- arXiv:0712.1937 [astro-ph].
- [90] L. Covi, M. Grefe, A. Ibarra, and D. Tran, “Neutrino Signals from Dark Matter Decay,” *JCAP* **1004** (2010) 017, arXiv:0912.3521 [hep-ph].
- [91] **IceCube** Collaboration, R. Abbasi *et al.*, “Search for Dark Matter from the Galactic Halo with the IceCube Neutrino Observatory,” *Phys.Rev.* **D84** (2011) 022004, arXiv:1101.3349 [astro-ph.HE].
- [92] A. Ibarra, D. Tran, and C. Weniger, “Indirect Searches for Decaying Dark Matter,” *Int.J.Mod.Phys.* **A28** no. 27, (2013) 1330040, arXiv:1307.6434 [hep-ph].
- [93] L. Hui, “Unitarity bounds and the cuspy halo problem,” *Phys.Rev.Lett.* **86** (2001) 3467–3470, arXiv:astro-ph/0102349 [astro-ph].
- [94] M. Kuhlen, P. Madau, and J. Silk, “Exploring Dark Matter with Milky Way substructure,” *Science* **325** (2009) 970–973, arXiv:0907.0005 [astro-ph.GA].